



Optimization of Electrospinning Parameters for Electrospun Nanofiber-Based Triboelectric Nanogenerators

Shin Jang¹ · Yeongjun Kim² · Samgon Lee³ · Je Hoon Oh²

Received: 15 January 2019 / Revised: 18 June 2019 / Accepted: 23 June 2019 / Published online: 16 July 2019
© Korean Society for Precision Engineering 2019

Abstract

In this study, the effects of various fabrication parameters on the electrical performance of an electrospun nanofiber-based triboelectric nanogenerator (EN-TENG) are systematically investigated through the design of experiments. We selected four fabrication parameters to examine, namely: (i) working distance (needle to collector distance), (ii) needle gauge, (iii) electrospinning time, and (iv) counter materials. A mixed orthogonal array of L_{18} experiments was designed with respect to the one factor having two level values and three factors having three level values. The open circuit voltage of the EN-TENG was varied from 86.1 to 576.7 V with the aforementioned fabrication parameters. A longer working distance, a larger needle gauge, and a longer electrospinning time increased the open circuit voltage. The power density of the optimized EN-TENG was approximately 2.39 W/m² at a 100 M Ω load resistance and was sufficient to illuminate a total of 200 LEDs.

Keywords Triboelectric nanogenerator · Electrospinning · P(VDF-TrFE) · Nanofibers · Design of experiments

List of Symbols

| | |
|--------------|--|
| ρ_A | Charge density on the surface of the contact materials |
| Q | Transferred charges |
| ϵ_0 | Relative permittivity of the air |
| ϵ_r | Relative permittivity of contact material |
| d | Thickness of the contact material |
| $x(t)$ | Distance variation between the contact materials |

1 Introduction

Since wearable electronics have gained much interest in recent years, simple, lightweight, and portable energy harvesters have become important. A nanogenerator that can sustainably harvest electric energy from environmental sources is a good candidate. Based on piezoelectric, pyroelectric, electromagnetic, and triboelectric mechanisms, a variety of nanogenerators have been intensively studied [1–4]. Among them, triboelectric nanogenerators (TENGs) have shown excellent electrical performance, simple configuration, low weight, and low fabrication cost compared to other types of nanogenerators. Depending on the design of the TENG structure, it is capable of harvesting various sustainable energy sources, such as human motion, walking, vibration, impact, wind, water waves, rain, and even heat [5–9].

TENGs are based on the coupling of the triboelectric effect and electrostatic induction, which causes charge transfer between two different contact materials when they come into contact with each other [10, 11]. For TENGs, the electrical performance and fabrication process are the two major concerns. To improve performance, the amount of charge generation between contact materials should be increased by properly selecting and manipulating the materials. Moreover, a simpler manufacturing process is preferred in terms of cost.

Shin Jang and Yeongjun Kim contributed equally to this work.

✉ Je Hoon Oh
jehoon@hanyang.ac.kr

¹ LC Technology Team, Samsung Display Co., LTD,
181, Samsung-ro, Tangjeong-myeon, Asan-Si,
Chungcheongnam-do 31454, Korea

² Department of Mechanical Engineering, Hanyang University,
55, Hanyangdaehak-ro, Ansan, Gyeonggi-do 15588, Korea

³ Commercial Vehicle Suspension and Steering
Engineering Design Team, Hyundai Motor Group,
150, Hyundaiyeonguso-ro, Namyang-eup, Hwaseong-Si,
Gyeonggi-do 18280, Korea

Poly(vinylidene fluoride-co-trifluoroethylene) (P(VDF-TrFE)) is a good triboelectric material that can easily gain electrons when it comes into contact with another material that loses electrons [12]. Moreover, it has been intensively used for TENGs as a contact material due to its ease of handling, low toxicity, and flexible mechanical properties. Electrospinning could be the best approach for manipulating the P(VDF-TrFE) structure, as this process is able to directly produce long and thin nanofibers continuously [13, 14]. In electrospinning, a polymer solution is ejected from a nozzle tip by applying a high electric potential difference between the nozzle and a grounded collector. After ejection, the jet experiences a whipping instability and extension before deposition due to interactions between charges existing on the jet, resulting in micro- and nanofibers. The electrospun fibers have a rough surface and remarkably large surface area per unit volume. It has been demonstrated that electrospun fibers can improve the triboelectric effect, and their large surface area allows the generation of more charges [15–18].

To date, many TENGs fabricated via electrospinning have been reported based on various structures, mechanisms, and materials. Zheng et al. compared the electrical performance of TENGs fabricated by electrospun poly(vinylidene fluoride) (P(VDF)) nanofibers and P(VDF) films [19]. Huang et al. also utilized electrospinning to fabricate P(VDF) nanofiber-based TENGs and noted that secondary-nanostructured nanofibers could enhance electrical performance [20]. Ye et al. showed that poly(vinylidene fluoride-co-hexafluoropropylene) (P(VDF-HFP)) nanofibers produced by electrospinning can improve the electrical performance of TENGs [21]. Our group has demonstrated that honeycomb-like nanofibers can enhance the electrical performance of TENGs further, and the effect of P(VDF-TrFE) concentration was investigated [22]. More recently, polymer nanocomposites have been fabricated as nanofibers or foam layer for TENGs [12, 23–28]. Nevertheless, the fabrication process is not well optimized, and the electrical performance of TENGs based on nanofibers is still insufficient for use in practical applications. Moreover, a design of experiments (DOE) methodology has not been applied to the fabrication of TENGs even though it is a proven way to improve electrical performance [29].

In this study, the effects of various parameters on the electrical performance of electrospun nanofiber-based TENGs (EN-TENGs) are systematically investigated through DOE. We selected four fabrication parameters: (i) working distance (needle to collector distance), (ii) needle gauge (inner diameter of the needle), (iii) electrospinning time, and (iv) counter materials. A mixed orthogonal array of L_{18} experiments was designed with respect to one factor having two level values and three factors having three level values. The electrical performance of EN-TENGs was affected by all the electrospinning parameters mentioned above, especially

the working distance. An EN-TENG was fabricated with the optimized parameters, and the electrical performances such as open circuit voltage, short circuit current, and power density under various load resistances were measured. The performances were also demonstrated by illuminating a few hundred light-emitting diodes (LEDs) and applying it as a finger motion detector.

2 Methods

2.1 Materials

A commercial P(VDF-TrFE) (70:30) powder was purchased from Piezotech. To prepare electrospinning inks, the P(VDF-TrFE) powder was dissolved in dimethylformamide (DMF, Sigma Aldrich) and acetone (Samcheon Chemical) for 12 h using a magnetic stirrer. The concentration of P(VDF-TrFE) was fixed to 15 wt %, and the volume ratio between DMF and acetone was set to 7:3 for inks. An indium-tin-oxide polyethylene terephthalate (ITO-PET) film was used as a collector. As counter contact materials for the evaluation of the EN-TENGs, aluminum (Al), polyimide (PI), and nylon (Ny) were prepared. The thickness of Al, PI, and Ny measured with a micrometer were 100 μm , 150 μm , and 50 μm , respectively.

2.2 Electrospinning Process

Electrospinning was performed with an in-house system, as shown in Fig. 1. A nozzle was connected to an adaptor that acts as an upper electrode, and a high-voltage supply (FJ50P2.5, Glassman) was used to apply high electric

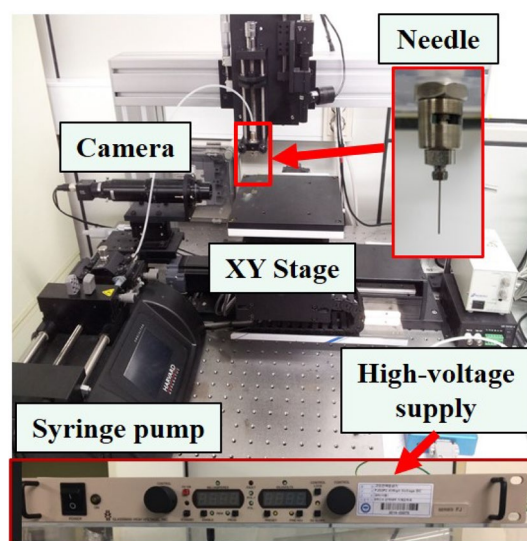


Fig. 1 In-house electrospinning system and each part

potentials to the P(VDF-TrFE) ink. ITO-PET was ultrasonicated in deionized water for 5 min to remove surface contamination. ITO-PET was then placed on the ground electrode connected to the work plate. For all experiments, P(VDF-TrFE) ink was fed into the nozzle using a syringe pump (PHD Ultra, Harvard Apparatus) with a fixed flow rate of 8 $\mu\text{l}/\text{min}$. The driving voltage was set to 10 kV. 24 G, 25 G, and 27 G needles with inner diameters of 310 μm , 260 μm , and 210 μm , respectively, were used. Electrospinning time was varied from 1 to 3 h with an interval of 1 h. The working distance was set to 100 mm and 150 mm. The ambient humidity was controlled below 30% by using a dehumidifier (NE-45ND, Nawoo).

2.3 Fabrication and Evaluation of EN-TENGs

Figure 2 shows the simple fabrication process of EN-TENGs. The electrospun P(VDF-TrFE) nanofibers onto ITO-PET ($40 \times 40 \text{ mm}^2$) themselves were used as a contact material without any post-processing, such as transferring the nanofibers to another substrate. A counter material connected to an in-house actuating system was placed above the nanofibers. The contact and separation process between nanofibers and the counter material was actuated by the system controlled via LabVIEW, as shown in Fig. 3a. The contact force was recorded through a load cell (UMM-K20, Dacell) and a data acquisition board (PXIe-4330, National Instruments) mounted on a PXI chassis with a controller (PXIe-8135 and PXIe-1082, National Instruments). The applied force and contact frequency were fixed at $\sim 10 \text{ N}$ and 2 Hz, respectively. The open circuit voltage and short circuit current were measured using an oscilloscope (MDO-3012, Tektronix) and a preamplifier (SR570, Stanford Research Systems). The microstructure was observed by a field-emission scanning electron microscope (FE-SEM: S-4800, Hitachi). The needle gauge and counter materials, as shown in Fig. 3b, c, were used to evaluate the electrical performance of the EN-TENGs. The working distance was set to 100 mm and 150 mm.

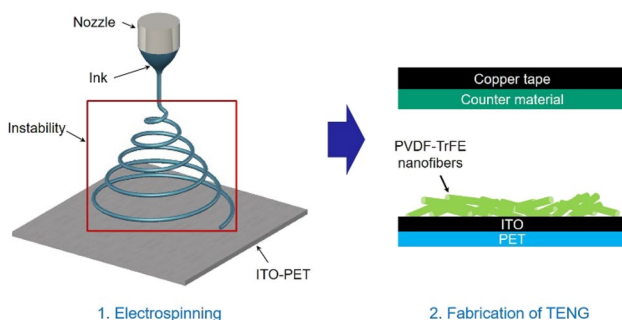


Fig. 2 A schematic of the fabrication procedure for EN-TENG via electrospinning

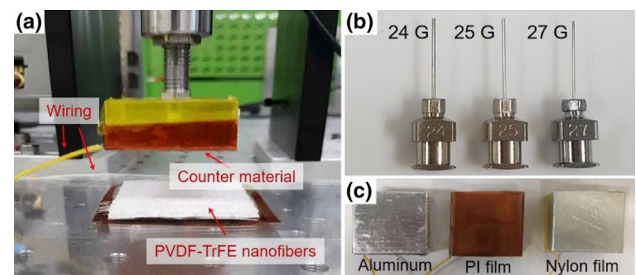


Fig. 3 a In-house actuating system, b needles for electrospinning, c counter materials

3 Results and Discussion

3.1 Electrospun P(VDF-TrFE) Nanofibers

The major parameters investigated in this study were selected based on fabrication parameters for electrospinning and TENGs. Even though the electrospinning process is relatively easy and simple, the mechanism is complex and not fully understood because there are a variety of parameters, including ink properties (surface tension, viscosity, conductivity, dielectric properties, solvent evaporation), processing conditions (needle gauge, configuration, and shape, electrospinning time, applied voltage, flow rate, working distance, collectors), and ambient conditions (humidity and temperature). As the material properties and other parameters have already been investigated by our group [13, 22], we selected continuous variables of working distance, needle gauge, and electrospinning time. In addition, the counter material for electrospun P(VDF-TrFE) nanofibers was considered to be a TENG fabrication parameter. It should be noted that counter material is a discrete variable. A total of four factors having different level values were chosen (Table 1). A mixed orthogonal array of L_{18} experiments was then designed, as shown in Table 2 [30, 31]. Eighteen EN-TENGs were fabricated and evaluated according to the variables. The open circuit voltages of three samples were measured for each case. Contact and separation cycles were repeated 20 times for each sample

Table 1 Selection of fabrication parameters

| Fabrication parameters | Level values | | |
|-------------------------|--------------|-----------|-------|
| | 1 | 2 | 3 |
| A: working distance | 100 mm | 150 mm | |
| B: needle gauge | 24 G | 25 G | 27 G |
| C: electrospinning time | 1 h | 2 h | 3 h |
| D: counter material | Aluminum | Polyimide | Nylon |

Table 2 A mixed orthogonal array of L18 experiments and the averaged open circuit voltage of three samples per each experiment

| No. | A (mm) | B (G) | C (h) | D | Open circuit voltage (V) | | |
|-----|--------|-------|-------|----|--------------------------|-------|-------|
| 1 | 100 | 24 | 1 | Al | 86.9 | 86.8 | 84.5 |
| 2 | 100 | 24 | 2 | PI | 419.6 | 468.0 | 462.4 |
| 3 | 100 | 24 | 3 | Ny | 249.2 | 232.2 | 254.4 |
| 4 | 100 | 25 | 1 | Al | 225.2 | 245.6 | 221.4 |
| 5 | 100 | 25 | 2 | PI | 428.0 | 428.0 | 437.3 |
| 6 | 100 | 25 | 3 | Ny | 284.0 | 276.0 | 308.0 |
| 7 | 100 | 27 | 1 | PI | 488.0 | 500.0 | 486.7 |
| 8 | 100 | 27 | 2 | Ny | 306.7 | 320.0 | 334.7 |
| 9 | 100 | 27 | 3 | Al | 254.0 | 262.7 | 263.3 |
| 10 | 150 | 24 | 1 | Ny | 296.0 | 306.7 | 318.6 |
| 11 | 150 | 24 | 2 | Al | 264.0 | 269.3 | 274.6 |
| 12 | 150 | 24 | 3 | PI | 530.7 | 528.0 | 524.0 |
| 13 | 150 | 25 | 1 | PI | 431.6 | 468.4 | 421.6 |
| 14 | 150 | 25 | 2 | Ny | 259.0 | 307.8 | 306.4 |
| 15 | 150 | 25 | 3 | Al | 337.8 | 353.2 | 374.6 |
| 16 | 150 | 27 | 1 | Ny | 226.4 | 253.0 | 268.6 |
| 17 | 150 | 27 | 2 | Al | 218.2 | 225.0 | 234.0 |
| 18 | 150 | 27 | 3 | PI | 609.0 | 571.0 | 550.0 |

and these values were averaged. It should be noted that 54 cases are required for the full factorial experiment.

All EN-TENGs fabricated in this study were evaluated and characterized in contact-separation mode [22]. Figures 4a, b show the electric circuit and open circuit voltage of EN-TENGs corresponding to the contact and separation of the contact materials. Initially, no electric charges in the materials were found because there is no contact between the nanofibers and counter material (Fig. 5a). When two friction materials come into contact, charges are generated on the material surfaces. One material loses electrons, and the other gains electrons. In this step, all charges are ideally in the same plane; thus, the EN-TENG is in an electrically neutral state (Fig. 5b). As the materials are separated (releasing and fully released), the system is no longer in electrical equilibrium, allowing the free electrons in the electrode attached to the contact material to move toward equilibrium (Figs. 5c, d). When the materials are pressed into contact again, the free electrons return to their original position (Fig. 5e). Through this process, AC electrical output is obtained, as shown in Fig. 4. Furthermore, voltage or current is observed depending on the electrical wiring of a load resistor between the two electrodes.

Before analyzing the open circuit voltage of the EN-TENGs, the effects of working distance and needle gauge on nanofiber structure were evaluated. Figure 6 shows the surface of P(VDF-TrFE) nanofiber mats according to working distance and needle gauge. To investigate the effect of working distance, the needle gauge and electrospinning time were fixed at 24 G and 2 h, respectively (Fig. 6a, b). As can be seen in the images, there was no difference on the surface

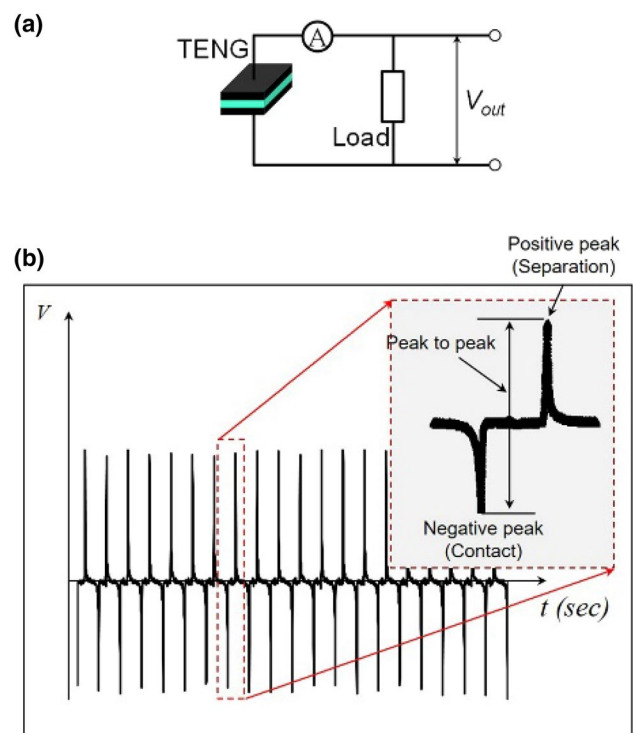


Fig. 4 a Electric circuit for TENG evaluation and b open circuit voltage corresponding to the contact and separation between P(VDF-TrFE) nanofibers and a counter material

morphology of each nanofiber mat. We also confirmed the effect of the needle gauge on the nanofiber structures with nanofibers electrospun for 2 h at the working distance of 100 mm (Fig. 6c–e). Similar to the working distance, there

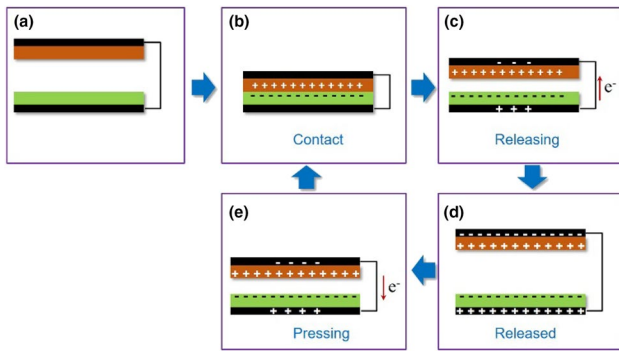


Fig. 5 Illustration of the operating mechanism of contact-separation mode TENGs: **a** initial, **b** contact, **c** releasing, **d** fully released, and **e** pressing states

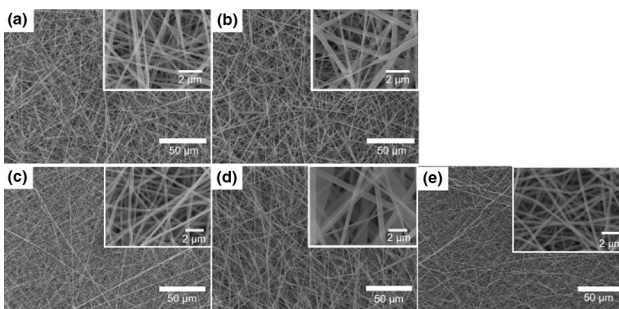


Fig. 6 Effect of working distance: **a** 100 mm and **b** 150 mm, and needle gauges: **c** 24 G, **d** 25 G, and **e** 27 G, on the microstructure of electrospun P(VDF-TrFE) nanofiber mats

was no significant difference in the microstructure with different needle gauges. In this study, three needle gauges, 24 G, 25 G, and 27 G, were used to produce P(VDF-TrFE) nanofibers, with inner diameters of the needles of 310 μm, 260 μm, and 210 μm, respectively. Even though the diameter of the 24 G needle is larger than that of a 27 G needle, the size of the nanofiber was not significantly changed.

Nanofiber mat thickness was also measured using a micrometer to investigate the effect of electrospinning time, working distance, and needle gauge. As expected, the thickness of the nanofiber mats was noticeably increased with increasing electrospinning time (Fig. 7a).

As the electrospinning time increased, the thickness of the nanofiber increased. However, when electrospinning was performed for longer than 3 h, the fabricated fibers piled up at a random point and hardened. This phenomenon not only significantly degrades the performance of the TENG but also prevents the counter materials from having even contact with the nanofiber layer due to its stiffness. We also investigated the effect of the needle gauge on the thickness of the nanofibers (Fig. 7b). As can be seen from the graph, the thickness increased as the gauge increased. In addition, the working

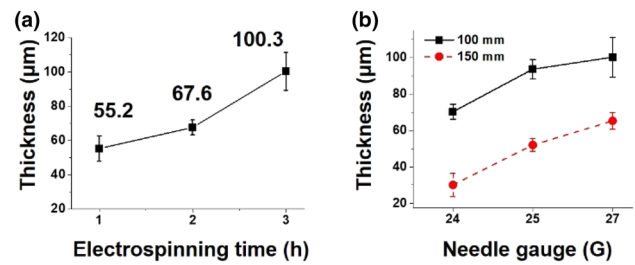


Fig. 7 Thickness of nanofiber mats with respect to **a** electrospinning time and **b** needle gauge. Error bars indicate standard deviation of three samples

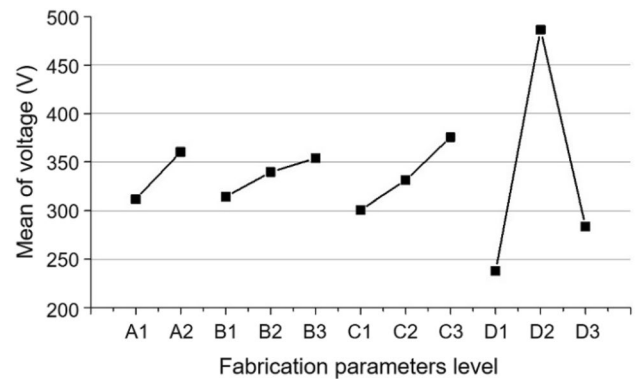


Fig. 8 Main effect plots for levels of parameters

distance dramatically affects the thickness of the nanofiber. However, the difference between 25 G and 27 G was not significant, and a severe clogging problem occurs when using a needle with a smaller diameter than 27 G.

3.2 Evaluation of EN-TENGs

EN-TENGs were fabricated and evaluated according to the designed L_{18} experiments (Table 2). The main effect plots for working distance, needle gauge, electrospinning time, and counter material are shown in Fig. 8. Open circuit voltage was used as a performance index of TENGs because high open circuit voltage leads to high power density [17, 32, 33]. All the parameters affect the open circuit voltage of the EN-TENGs. For the performance of TENGs, the output voltage of a typical TENG operated in contact-separation mode is determined as follows [11]:

$$V = \frac{\rho_A \cdot x(t)}{\epsilon_0} - \frac{Q}{S\epsilon_0} \left(\frac{d_1}{\epsilon_{r1}} + \frac{d_2}{\epsilon_{r2}} + x(t) \right) \tag{1}$$

where ρ_A , Q , ϵ_{r1} , ϵ_{r2} , and S are the charge density on the surface of the contact materials, transferred charges, relative permittivity of each contact material, and surface area, respectively. d and $x(t)$ denote thickness and distance

variation between the contact materials, respectively. In particular, open circuit voltage is linearly proportional to the product of ρ_A and $x(t)$ because Q is negligible.

All three electrospinning parameters showed significant effects on the performance of nanofiber-based TENGs. The thickness of the nanofiber mat increased with increasing the electrospinning time and needle gauge. Charges in porous media are induced not only on the surface of the electrospun nanofiber mat but also on the surfaces of the inner fibers by electrostatic induction. Thus, ρ_A becomes higher at thicker porous media. On the contrary, $x(t)$ decreases as the thickness of nanofiber mat increases. Since the increase in ρ_A would be much more significant than the decrease in $x(t)$, open circuit voltage tends to rise with increasing the thickness of nanofiber mat resulted from the increasing electrospinning time and needle gauge.

In contrast, the opposite tendency was observed for the effect of working distance. The nanofiber mat produced at a shorter distance of 100 mm was thicker, but a lower open circuit voltage was generated. The size and structure of produced nanofibers might cause this opposite tendency.

Table 3 Result of analysis of variance (ANOVA) test

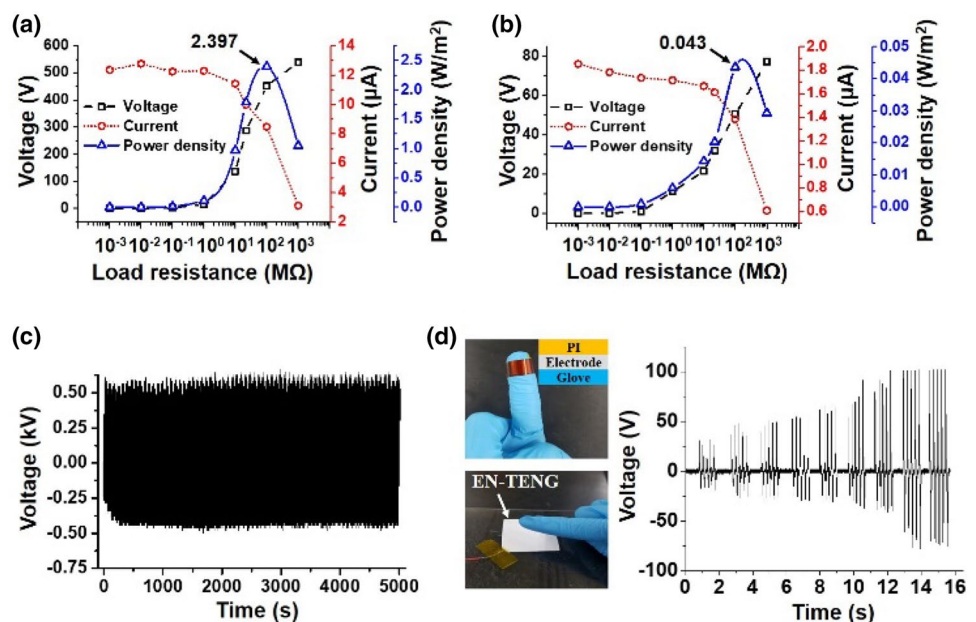
| Factor | S | Φ | V (=S/ Φ) | F_0 | P |
|-----------|---------|--------|-----------------|--------|-------|
| A | 31,969 | 1 | 31,969 | 16.20 | 0.000 |
| B | 14,589 | 2 | 7295 | 3.70 | 0.032 |
| C | 50,921 | 2 | 25,461 | 12.90 | 0.000 |
| D | 628,852 | 2 | 314,426 | 159.36 | 0.000 |
| Error (e) | 90,759 | 46 | 1973 | | |
| T | 817,091 | 53 | | | |

At a longer working distance, the diameter of electrospun nanofibers tends to decrease especially at the beginning of the electrospinning process, and the electrospun nanofiber mat has much denser structures [34–36]. It would be expected that denser nanofiber structures with a smaller fiber diameter were fabricated at the working distance of 150 mm. Since denser nanofiber structures near the surface can induce more charges, ρ_A becomes higher at a longer working distance even though the nanofiber mat has a smaller thickness. As mentioned above, open circuit voltage is dominantly influenced by ρ_A , so higher open circuit voltage was obtained at a longer working distance.

Although open circuit voltage of EN-TENGs is determined by the product of ρ_A and $x(t)$, the effect of ρ_A is much more dominant than that of $x(t)$. ρ_A of the nanofiber mat could be enhanced by a longer electrospinning time, a larger needle gauge, and a longer working distance, thus resulting in improved open circuit voltages. Based on the main effect plot and ANOVA (Table 3), all three electrospinning parameters were found to be statistically significant (P value < 0.05). The selection of contact materials was also strongly related to the performance of TENGs. ANOVA confirms that the counter material was the most dominant parameter. It is consistent with the well-known triboelectric series.

We also conducted additional experiments to compare the best set of parameters with the worst one (Fig. 9a, b). To avoid interference of the counter materials, we used PI as the counter material for both sets. The best conditions of working distance, needle gauge, and electrospinning time were 150 mm, 27 G, and 3 h, respectively, and the corresponding worst sets were selected to be 100 mm, 24 G, and

Fig. 9 Voltage, current, and power density of the EN-TENGs with **a** the best and **b** the worst fabrication parameter sets under load resistance. Continuous open circuit voltage output with **c** a motorized tapping machine and **d** finger tapping



1 h. The maximum open circuit voltage was measured to be 578 V and 101 V for the best and worst sets, respectively. We also measured the power density under load resistance, which showed 2.39 W/m² and 0.0436 W/m² at 100 MΩ. The maximum open circuit voltage and power density could be improved by 5.7 times and 54.8 times, respectively, by controlling the electrospinning parameters. Indeed, the difference in open circuit voltage was remarkably large, even though only three electrospinning parameters were considered. Moreover, the performance of the best set is comparable to the EN-TENG fabricated in an earlier study, and it shows a more than twofold increase [22]. It is worth noting that further improvement is possible by considering more parameters with DOE.

With the best parameters, we carried out two sets of confirmatory experiments. The EN-TENG was continuously pressed and released for 5000 s at 2 Hz to investigate the feasibility, and it showed approximately the same open circuit voltage during the whole test (Fig. 9c). We also demonstrated the dynamic energy harvest with a finger-attached device. As shown in Fig. 9d, we attached a 10 mm by 10 mm electrode and PI film on a glove and consecutively tapped an electrospun P(VDF-TrFE) nanofiber. Several sets of tapping were conducted with increasing pressure, and the nanofiber was tapped five times with a similar pressure at each set. As can be seen from the graph, the EN-TENG harvested electric energy from each tap well.

3.3 Demonstration of EN-TENGs

The performance of the best EN-TENG was demonstrated by charging capacitors and lighting 200 light-emitting diodes (LEDs) which have a turn-on voltage of ~3.2 V. Figure 10a shows a full-wave rectifier bridge to convert AC output to DC output. A 0.47 μF capacitor was charged to 50 V within 200 s at a frequency of 2 Hz; for 2.2 μF, 10 μF, 22 μF, 100 μF, and 330 μF capacitors, the charging slopes were 0.174 V/s, 0.0394 V/s, 0.0309 V/s, 0.00708 V/s, and 0.00202 V/s, respectively (Fig. 10b). At the same operating conditions, we could instantaneously turn on 200 blue LEDs by the produced output voltage of the EN-TENG, as shown in Fig. 10c. From this demonstration, it would be expected that well-optimized process conditions and a properly chosen counter material could greatly enhance the performance of TENGs, and the proposed EN-TENG could be applied to a green energy harvester.

4 Conclusions

We investigated the effects of various parameters on the electrical performance of electrospun nanofiber-based TENGs (EN-TENGs) via DOE. We selected four fabrication

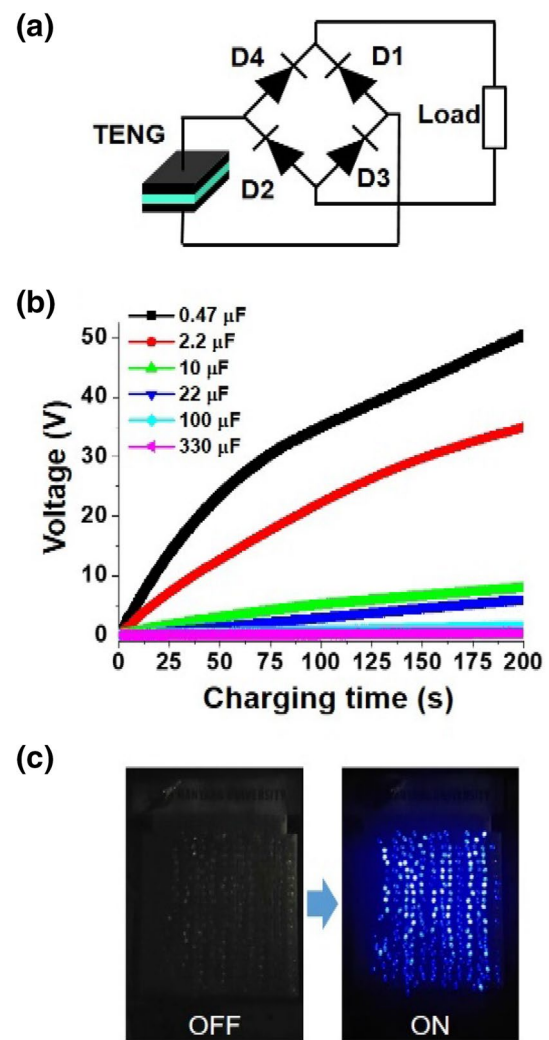


Fig. 10 Demonstration of the optimized EN-TENG: **a** electric circuit for various applications, **b** charging of various capacitors, and **c** illumination of 200 LEDs

parameters, namely: working distance, needle gauge, electrospinning time, and contact material. A mixed orthogonal array of L_{18} experiments was designed concerning one factor having two level values and three factors having three level values. All parameters were statistically significant (P value < 0.05) based on the main effect plot and ANOVA test. Among the three electrospinning parameters, working distance and electrospinning time showed more significant influences on the performance of EN-TENGs. A longer working distance would increase the charge density of the nanofiber mat due to its thin nanofibers and compact structures, resulting in improved electrical performance. The paring of contact material based on the triboelectric series also had a significant effect. EN-TENG showed the highest performance when working distance, needle gauge, and electrospinning time were 150 mm, 27 G, and 3 h, respectively.

It was shown that adoption of the DOE methodology could increase the open circuit voltage of EN-TENGs by more than 6.7 times from 86.1 V to 576.7 V. The EN-TENG fabricated with the best process conditions and PI as a counter material showed a power density of 2.39 W/m². It was able to harvest electric energy during 10,000 cycles stably and even from finger tapping. We confirmed that the EN-TENG could be applied in various applications, such as capacitor charging and LED illumination.

Acknowledgements This work was supported by a National Research Foundation of Korea (NRF) grant funded by the Korean government (MSIP) (No. 2019R1A2C1005023).

Compliance with Ethical Standards

Conflict of interest On behalf of all authors, the corresponding author states that there is no conflict of interest.

References

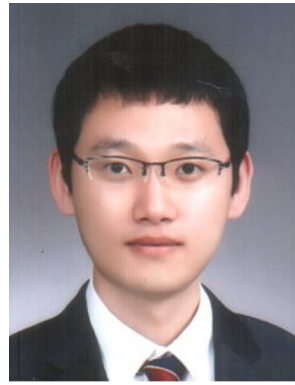
- Izhar, Khan F. U. (2018). Three degree of freedom acoustic energy harvester using improved helmholtz resonator. *Int J Precis Eng Manuf*, 19(1), 143–154.
- Park, H. (2017). Vibratory electromagnetic induction energy harvester on wheel surface of mobile sources. *Int J Precis Eng Manuf Green Tech*, 4(1), 59–66.
- Jang, S., & Oh, J. H. (2018). Rapid fabrication of microporous BaTiO₃/PDMS nanocomposites for triboelectric nanogenerators through one-step microwave irradiation. *Sci Rep*, 8, 14287.
- Cao, L., Li, Z., Guo, C., Li, P., Meng, X., & Wang, T. (2019). Design and test of the MEMS coupled piezoelectric-electromagnetic energy harvester. *Int J Precis Eng Manuf*, 20(4), 673–686.
- Wang, Z. L. (2013). Triboelectric nanogenerators as new energy technology for self-powered systems and as active mechanical and chemical sensors. *ACS Nano*, 7(11), 9533–9557.
- Yang, Y., Zhu, G., Zhang, H., Chen, J., Zhong, X., Lin, Z.-H., et al. (2013). Triboelectric nanogenerator for harvesting wind energy and as self-powered wind vector sensor system. *ACS Nano*, 7(10), 9461–9468.
- Lee, J.-H., Ryu, H., Kim, T.-Y., Kwak, S.-S., Yoon, H.-J., Kim, T.-H., et al. (2015). Thermally induced strain-coupled highly stretchable and sensitive pyroelectric nanogenerators. *Adv Energy Mater*, 5, 1500704.
- Jang, S., Kim, H., & Oh, J. H. (2017). Simple and rapid fabrication of pencil-on-paper triboelectric nanogenerators with enhanced electrical performance. *Nanoscale*, 9, 13034–13041.
- Zhu, G., Lin, Z.-H., Jing, Q., Bai, P., Pan, C., Yang, Y., et al. (2013). Toward large-scale energy harvesting by a nanoparticle-enhanced triboelectric nanogenerator. *Nano Lett*, 13, 847–853.
- Fan, F.-R., Lin, L., Zhu, G., Wu, W. Z., Zhang, R., & Wang, Z. L. (2012). Transparent triboelectric nanogenerators and self-powered pressure sensors based on micropatterned plastic films. *Nano Lett*, 12, 3109–3114.
- Niu, S., Wang, S., Lin, L., Liu, Y., Zhou, Y. S., Hu, Y., et al. (2013). Theoretical study of contact-mode triboelectric nanogenerators as an effective power source. *Energy Environ Sci*, 6, 3576–3583.
- Wang, X., Yang, B., Liu, J., Zhu, Y., Yang, C., & He, Q. (2016). A flexible triboelectric-piezoelectric hybrid nanogenerator based on P(VDF-TrFE) nanofibers and PDMS/MWCNT for wearable devices. *Sci Rep*, 6, 36409.
- Jang, S., Kim, Y., & Oh, J. H. (2016). Influence of processing conditions and material properties on electrohydrodynamic direct patterning of a polymer solution. *J Electron Mater*, 45(4), 2291–2298.
- Cho, Y. S., Lee, J. S., Hong, M. W., Lee, S.-H., Kim, Y. Y., & Cho, Y.-S. (2018). Comparative assessment of the ability of dual-pore structure and hydroxyapatite to enhance the proliferation of osteoblast-like cells in well-interconnected scaffolds. *Int J Precis Eng Manuf*, 19(4), 605–612.
- Chen, F., Wu, Y., Ding, Z., Xia, X., Li, S., Zheng, H., et al. (2019). A novel triboelectric nanogenerator based on electrospun polyvinylidene fluoride nanofibers for effective acoustic energy harvesting and self-powered multifunctional sensing. *Nano Energy*, 56, 241–251.
- Garain, S., Jana, S., Sinha, T. K., & Mandal, D. (2016). Design of in situ Poled Ce³⁺-doped electrospun PVDF/graphene composite nanofibers for fabrication of nanopressure sensor and ultrasensitive acoustic nanogenerator. *ACS Appl Mater Interfaces*, 8, 4532–4540.
- Mi, H.-Y., Jing, X., Zheng, Q., Fang, L., Huang, H.-X., Turng, L.-S., et al. (2018). High-performance flexible triboelectric nanogenerator based on porous aerogels and electrospun nanofibers for energy harvesting and sensitive self-powered sensing. *Nano Energy*, 48, 327–336.
- Li, Z., Shen, J., Abdalla, I., Yu, J., & Ding, B. (2017). Nanofibrous membrane constructed wearable triboelectric nanogenerator for high performance biomechanical energy harvesting. *Nano Energy*, 36, 341–348.
- Zheng, Y., Cheng, L., Yuan, M., Wang, Z., Zhang, L., Qin, Y., et al. (2014). An electrospun nanowire-based triboelectric nanogenerator and its application in a fully self-powered UV detector. *Nanoscale*, 6, 7842–7846.
- Huang, T., Wang, C., Yu, H., Wang, H., Zhang, Q., & Zhu, M. (2015). Human walking-driven wearable all-fiber triboelectric nanogenerator containing electrospun polyvinylidene fluoride piezoelectric nanofibers. *Nano Energy*, 14, 226–235.
- Ye, B. U., Kim, B.-J., Ryu, J., Lee, J. Y., Baik, J. M., & Hong, K. (2015). Electrospun Ion gel nanofibers for flexible triboelectric nanogenerator: electrochemical effect on output power. *Nanoscale*, 7, 16189–16194.
- Jang, S., Kim, H., Kim, Y., Kang, B. J., & Oh, J. H. (2016). Honeycomb-like nanofiber based triboelectric nanogenerator using self-assembled electrospun poly(vinylidene fluoride-co-trifluoroethylene) nanofibers. *Appl Phys Lett*, 108, 143901.
- Lee, D., Chung, J., Yong, H., Lee, S., & Shin, D. (2019). A deformable foam-layered triboelectric tactile sensor with adjustable dynamic range. *Int J Precis Eng Manuf Green Tech*, 6(1), 43–51.
- Wang, H., Shi, M., Zhu, K., Su, Z., Cheng, X., Song, Y., et al. (2016). High performance triboelectric nanogenerators with aligned carbon nanotubes. *Nanoscale*, 8, 18489–18494.
- Chen, J., Guo, H., He, X., Liu, G., Xi, Y., Shi, H., et al. (2016). Enhancing performance of triboelectric nanogenerator by filling high dielectric nanoparticles into sponge PDMS film. *ACS Appl Mater Interfaces*, 8, 736–744.
- He, X., Guo, H., Yue, X., Gao, J., Xi, Y., & Hu, C. (2015). Improving energy conversion efficiency for triboelectric nanogenerator with capacitor structure by maximizing surface charge density. *Nanoscale*, 7, 1896–1903.
- Seung, W., Yoon, H.-J., Kim, T. Y., Ryu, H., Kim, J., Lee, J.-H., et al. (2017). Boosting power-generating performance of triboelectric nanogenerators via artificial control of ferroelectric polarization and dielectric properties. *Adv Energy Mater*, 7, 1600988.

28. Kwon, Y. H., Shin, S.-H., Kim, Y.-H., Jung, J.-Y., Lee, M. H., & Nah, J. (2016). Triboelectric contact surface charge modulation and piezoelectric charge induction using polarized composite thin film for performance enhancement of triboelectric generators. *Nano Energy*, 25, 225–231.
29. Song, J., Xie, H., Wu, W., Joseph, V. R., Wu, C. F. J., & Wang, Z. L. (2010). Robust optimization of the output voltage of nanogenerators by statistical design of experiments. *Nano Res*, 3(9), 613–619.
30. Karthikeyan, P., & Mahadevan, K. (2015). Investigation on the effects of sic particle addition in the weld zone during friction stir welding of Al 6351 alloy. *Int J Adv Manuf Technol*, 80, 1919–1926.
31. Tosun, N., Cogun, C., & Tosun, G. (2004). A study on kerf and material removal rate in wire electrical discharge machining based on taguchi method. *J Mater Process Technol*, 152, 316–322.
32. Wang, J., Wu, C., Dai, Y., Zhao, Z., Wang, A., Zhang, T., et al. (2017). Achieving ultrahigh triboelectric charge density for efficient energy harvesting. *Nat Commun*, 8(1), 88.
33. Zheng, Q., Fang, L., Guo, H., Yang, K., Cai, Z., Meador, M. A. B., et al. (2018). Highly porous polymer aerogel film-based triboelectric nanogenerators. *Adv Funct Mater*, 28, 1706365.
34. Baker, S. C., Atkin, N., Gunning, P. A., Granville, N., Wilson, K., Wilson, D., et al. (2006). Characterisation of electrospun polystyrene scaffolds for three-dimensional in vitro biological studies. *Biomaterials*, 27(16), 3136–3146.
35. Yuan, X., Zhang, Y., Dong, C., & Sheng, J. (2004). Morphology of ultrafine polysulfone fibers prepared by electrospinning. *Polym Int*, 53(11), 1704–1710.
36. Zhou, F.-L., Gong, R.-H., & Porat, I. (2010). Needle and needleless electrospinning for nanofibers. *J Appl Polym Sci*, 115, 2591–2598.

Publisher's Note Springer Nature remains neutral with regard to jurisdictional claims in published maps and institutional affiliations.



Shin Jang received his B.S., M.S. and Ph.D. degrees in Mechanical Engineering from Hanyang University, Korea. He is currently working for Samsung Display as a senior engineer.



Yeongjun Kim received his B.S. and M.S. degrees in mechanical engineering from Hanyang University, Korea. He is currently studying towards his Ph.D. degree in Mechanical Engineering at Hanyang University. His research interests include composite materials-based nanogenerators and porous elastomer-based pressure sensors.



Samgon Lee received his B.S. and M.S. degrees in Mechanical Engineering from Hanyang University, Korea. He is currently working for Hyundai Motor Group as a research engineer.



Je Hoon Oh received the B.S., M.S., and Ph.D. degrees in Mechanical Engineering from KAIST, Korea. He joined Hanyang University, Korea in 2004, and is currently a professor of Mechanical Engineering. His current research interests are in mechanical design, analysis of bolted joints, solution printing based electronic devices, energy harvester, and hemodynamics.